

RESEARCH

Open Access



Inhibition of LRRK2 kinase activity promotes anterograde axonal transport and presynaptic targeting of α -synuclein

Charlotte F. Brzozowski^{1,2}, Baraa A. Hijaz¹, Vijay Singh¹, Nolwazi Z. Gcwensa¹, Kaela Kelly³, Edward S. Boyden^{4,5,6}, Andrew B. West³, Deblina Sarkar⁷ and Laura A. Volpicelli-Daley^{1*} 

Abstract

Pathologic inclusions composed of α -synuclein called Lewy pathology are hallmarks of Parkinson's Disease (PD). Dominant inherited mutations in leucine rich repeat kinase 2 (LRRK2) are the most common genetic cause of PD. Lewy pathology is found in the majority of individuals with LRRK2-PD, particularly those with the G2019S-LRRK2 mutation. Lewy pathology in LRRK2-PD associates with increased non-motor symptoms such as cognitive deficits, anxiety, and orthostatic hypotension. Thus, understanding the relationship between LRRK2 and α -synuclein could be important for determining the mechanisms of non-motor symptoms. In PD models, expression of mutant LRRK2 reduces membrane localization of α -synuclein, and enhances formation of pathologic α -synuclein, particularly when synaptic activity is increased. α -Synuclein and LRRK2 both localize to the presynaptic terminal. LRRK2 plays a role in membrane traffic, including axonal transport, and therefore may influence α -synuclein synaptic localization. This study shows that LRRK2 kinase activity influences α -synuclein targeting to the presynaptic terminal. We used the selective LRRK2 kinase inhibitors, MLI-2 and PF-06685360 (PF-360) to determine the impact of reduced LRRK2 kinase activity on presynaptic localization of α -synuclein. Expansion microscopy (ExM) in primary hippocampal cultures and the mouse striatum, *in vivo*, was used to more precisely resolve the presynaptic localization of α -synuclein. Live imaging of axonal transport of α -synuclein-GFP was used to investigate the impact of LRRK2 kinase inhibition on α -synuclein axonal transport towards the presynaptic terminal. Reduced LRRK2 kinase activity increases α -synuclein overlap with presynaptic markers in primary neurons, and increases anterograde axonal transport of α -synuclein-GFP. *In vivo*, LRRK2 inhibition increases α -synuclein overlap with glutamatergic, cortico-striatal terminals, and dopaminergic nigral-striatal presynaptic terminals. The findings suggest that LRRK2 kinase activity plays a role in axonal transport, and presynaptic targeting of α -synuclein. These data provide potential mechanisms by which LRRK2-mediated perturbations of α -synuclein localization could cause pathology in both LRRK2-PD, and idiopathic PD.

Keywords: LRRK2, Parkinson's disease, α -synuclein, Trafficking, Presynaptic, Synapse, Axonal transport, Expansion microscopy

Introduction

Inclusions composed primarily of the protein, α -synuclein, found in axons, called Lewy neurites, and in the soma, called Lewy bodies [1], are among the primary hallmarks of PD. Mutations in LRRK2 cause familial PD, and increase its kinase activity. Gene variations in LRRK2 increase risk of developing sporadic PD [2, 3]. Increased

*Correspondence: lvolpicellidaley@uabmc.edu

¹ Department of Neurology, Center for Neurodegeneration and Experimental Therapeutics, University of Alabama at Birmingham, Birmingham, AL 35294, USA

Full list of author information is available at the end of the article



© The Author(s) 2021. **Open Access** This article is licensed under a Creative Commons Attribution 4.0 International License, which permits use, sharing, adaptation, distribution and reproduction in any medium or format, as long as you give appropriate credit to the original author(s) and the source, provide a link to the Creative Commons licence, and indicate if changes were made. The images or other third party material in this article are included in the article's Creative Commons licence, unless indicated otherwise in a credit line to the material. If material is not included in the article's Creative Commons licence and your intended use is not permitted by statutory regulation or exceeds the permitted use, you will need to obtain permission directly from the copyright holder. To view a copy of this licence, visit <http://creativecommons.org/licenses/by/4.0/>. The Creative Commons Public Domain Dedication waiver (<http://creativecommons.org/publicdomain/zero/1.0/>) applies to the data made available in this article, unless otherwise stated in a credit line to the data.

LRRK2 kinase activity has also been observed in post mortem tissue analysis of idiopathic PD brains [4]. Lewy pathology is common in individuals with PD harboring the most common G2019S-LRRK2 mutation, which is associated with increased nonmotor symptoms [5]. PD animal models demonstrate α -synuclein pathologic aggregation is exacerbated by G2019S-LRRK2 expression [6–11]. Given the importance of LRRK2 activity in both familial, and idiopathic PD cases, deciphering the downstream effects of LRRK2 kinase activity is crucial for investigating PD mechanisms, in general. An understanding of how LRRK2 kinase activity interacts with α -synuclein could help with determine how these two proteins contribute to LRRK2-PD, and idiopathic PD.

α -Synuclein is enriched in presynaptic terminals of glutamatergic neurons, and stabilizes synaptic vesicle SNARE formation via interactions with VAMP2, acting as a brake on synaptic vesicle exocytosis [12–17]. LRRK2 also plays a role in presynaptic vesicle traffic, and functionally interacts with presynaptic vesicle proteins [18–24]. One of the most well-established roles for LRRK2 is in membrane trafficking [25], and recent studies point to a role for LRRK2 in axonal transport in polarized neurons [26–28].

Association of α -synuclein with membranes in an alpha-helical, tetramer conformation in which the NAC domain is buried protects it from forming pathologic β -sheet aggregates [17, 29–34]. Altering the association of normal, tetrameric α -synuclein with membranes has been suggested as a therapeutic intervention against inclusion formation [30, 35–39]. G2019S-LRRK2 expression in neurons decreases membrane association of α -synuclein, suggesting a role in promoting α -synuclein aggregation [40]. Increasing neuronal activity in neurons expressing G2019S-LRRK2 reduces further exacerbates α -synuclein pathologic aggregation [41, 42]. Since α -synuclein primarily localizes to presynaptic vesicles [13, 43], it is possible that LRRK2 kinase activity plays a role in α -synuclein trafficking and localization to this compartment.

Here, we demonstrate using selective LRRK2 kinase inhibitors along with ExM, which provides exquisite resolution of synapses [44, 45], an increase in colocalization of α -synuclein with presynaptic markers. Reduction of LRRK2 kinase activity increases presynaptic targeting of α -synuclein in primary hippocampal neurons, and in glutamatergic and dopaminergic terminals in the mouse striatum. Inhibition of LRRK2 kinase activity also increases the motility and fast anterograde transport of α -synuclein along the axon. Together, our data suggest an interaction between LRRK2 kinase activity, and α -synuclein localization and targeting to presynaptic terminals. Moreover, they prompt further investigation into

the mechanisms by which LRRK2 kinase activity directs vesicular transport of α -synuclein along the axon and how that may influence pathology in LRRK2-PD, and idiopathic PD.

Materials and methods

Unless otherwise stated, all materials were purchased from Fisher Scientific.

Animals

All animal protocols were approved by the Institutional Animal Care and Use Committee at the University of Alabama at Birmingham. Pregnant CD1 mice were purchased from Charles River (Wilmington, MA). C57BL/6 J mice were from purchased from the Jackson Laboratory. PF-360 chow [46] was formulated at Research Diets Inc. Mice were on a 12-h light/dark cycle and had ad libitum access to food and water.

Primary hippocampal culture

Primary neuronal cultures from E16-E18 mouse embryos were generated as previously described [47]. Stocks of MLI-2 were prepared at 30 mM by dissolving in DMSO, and stored at -80°C for no more than 3 months (aliquots were not re-used). On DIV 7, neurons for immunoblotting, immunofluorescence, and ExM experiments were treated with LRRK2 inhibitor MLI-2 (10 nM or 30 nM respectively), or equivalent dilution of DMSO as control. Cells were lysed for western blot or fixed for immunofluorescence on DIV14.

Live cell imaging and kymograph analyses

Primary hippocampal neurons were transfected with 1.5 μg human α -synuclein-GFP plasmid DNA [48] using lipofectamine-LTX (ThermoFisher) on DIV6 and imaged on DIV10 using an inverted ZEISS Z1 Cell Observer fitted with a Colibri2 cool LED 5-channel fast wavelength switching system, and a Hamamatsu Orca Flash high-speed camera. The incubation chamber temperature was set at 32°C . Prior to recording, neuronal media was exchanged to pre-warmed imaging buffer (136 mM NaCl, 2.5 mM KCl, 2 mM CaCl_2 , 1.3 mM MgCl_2 , 10 mM glucose, 10 mM HEPES, pH 7.4) containing either 30 nM MLI-2 or DMSO control. Regions of thin axons at least 100 μm away from neurite tips, or adjacent cell bodies were chosen for imaging. The direction towards the cell soma was marked during recordings to help distinguish between anterograde (towards synaptic terminal) or retrograde (towards cell soma) direction during analysis. Images were captured every 300 ms for a total duration of 2 min. Kymographs were generated using the multi kymograph plugin in FIJI. Puncta count was determined by manual count within 50 μm of axon length. Mobile

puncta were defined by any kind of mobility throughout the recording window. To account for bidirectional travelling puncta, directionally mobile puncta were defined as those with a net vectorial movement of 10 μm in either retrograde or anterograde direction [49]. Net velocities of anterograde and retrograde trafficking were manually measured per each track by dividing the total distance travelled by total time travelled [50]. Only mobile puncta classified as either retrograde or anterograde were used to calculate overall velocity.

Immunoblots

Primary neurons were lysed on DIV14 using 2% SDS in Tris-buffered saline (TBS; 20 mM Tris, 150 mM NaCl, pH 7.4) containing phosphatase and protease inhibitors. Cells were scraped and sonicated for a total of 10 s (1 s on/off pulse, 30% amplitude). Lysates were centrifuged at 20,000 g, and the supernatant was diluted into 4X Laemmli buffer with 10% dithiothreitol. Protein lysates were electrophoresed on 8% (LRRK2) or 15% (α -synuclein) SDS-PAGE gels and transferred overnight onto PVDF membranes (Millipore). Blots were either blocked with Everyblot blocking reagent (BioRad) for LRRK2 and phospho-protein blots, or 5% milk in TBS-Tween followed by primary antibody incubation in blocking buffer overnight at 4 °C. The following antibodies were used: anti-LRRK2 c42-2 (Abcam, RRID: AB_2713963), anti-LRRK2 pS1292 (Abcam, RRID: AB_2732035), anti-LRRK2 pS935 (Abcam, RRID: AB_2732035), anti- α -synuclein (Abcam, RRID: AB_869971), anti-vGLUT1 (Synaptic Systems, RRID: AB_887878), anti-VAMP2 (Synaptic Systems, RRID: AB_887811), anti-dopamine transporter N-terminus rat monoclonal (RRID: AB_2190413), and anti-vinculin (Biorad, RRID: AB_2214389). Blots were then incubated with HRP-conjugated secondary antibodies (Jackson Immunoresearch) for 2 h at room temperature and developed with ECL (Biorad 40–720-71KIT). Blots were quantified using FIJI software.

Immunofluorescence

Transcardial perfusions

C57BL/6 J mice were transcardially perfused with 0.9% saline, 10 units/mL heparin, and sodium nitroprusside (0.5% w/v) followed by cold 4% paraformaldehyde (PFA), 30% acrylamide in phosphate buffered saline (PBS). After 12 h post fixation in 4% PFA at 4 °C, brains were embedded into a 2% agarose gel (in PBS). Agarose was dissolved in microwave-heated PBS and cooled down until 37 °C and then poured into a 6-well dish containing the brains followed by solidifying at 4 °C. A Leica VT1000 S was used to cut 100 μm thick brain sections which were stored in PBS at 4 °C. Sections were stored no longer than 2 weeks in PBS prior to IF processing.

Immunofluorescence Primary neurons

Neurons were fixed with a 4% PFA, 4% sucrose in PBS for 30 min at room temperature, rinsed five times in PBS, permeabilized and blocked with 0.05% saponin, 3% BSA in PBS. This buffer was used for the primary and secondary antibody incubations. The following antibodies were used: anti- α -synuclein (Abcam, RRID: AB_869971), anti-vGLUT1 (Synaptic Systems, RRID: AB_887878), anti-Homer1 (Synaptic Systems, RRID: AB_2631222). Primary incubations were performed at 4 °C overnight followed by five rinses. Samples were incubated in Alexa Fluor-conjugated secondary antibodies (ThermoFisher) for 1 h at room temperature, rinsed, and mounted onto glass slides (Superfrost Plus) in Prolong Gold (ThermoFisher).

Brain sections

Sections were rinsed three times in TBS, and then incubated in an antigen retrieval solution (10 mM sodium citrate, 0.05% Tween-20, pH 6.0) for 1 h at 37 °C. Sections were blocked and permeabilized for 1 h at 4 °C with agitation in 5% normal goat or donkey serum, 0.1% TritonX-100 in TBS. Primary antibodies were diluted 5% normal goat or donkey serum in TBS. The following antibodies were used: anti-total-synuclein (1:2000, RRID: AB_398107), anti-vGLUT1 (1:2000, RRID: AB_887878), anti-Homer1 (1:1000, RRID: AB_2631222), anti-hDAT-NT (1:5000, RRID: AB_2190413). Sections were incubated in Alexa-Fluor conjugated secondary antibodies diluted in 5% normal serum in PBS for 2 h at room temperature and mounted onto glass slides (Superfrost Plus) using Prolong gold (ThermoFisher).

Expansion microscopy

Primary neurons

Neurons were fixed and incubated with primary and secondary antibodies as described above. After secondary antibody incubations, neurons were anchored with succinimidyl ester of 6-((Acryloyl)amino) hexanoic acid (AcX) (ThermoFisher) in PBS (0.1 mg/ml) for 6 h at 4 °C. Samples were then incubated for 30 min at 37 °C in a gelling chamber containing the polymer solution (2 M NaCl, 8.625% sodium acrylate (Sigma), 2.5% acrylamide (Sigma), 0.15%N,N'-methylenebisacrylamide, 0.02% ammonium persulfate (Biorad), 0.02% TEMED (Biorad) in PBS) as described in [51] and [52]. To allow equidistant expansion, gelled coverslips were transferred into digestion solution (50 mM Tris, 1 mM EDTA, 1% Triton X-100, 0.8 M guanidine HCl, pH8) containing proteinase K (800 u/mL, NE) and incubated for 6 h at room temperature. After digestion, gel-embedded neurons were transferred to glass bottom imaging plates (Cellvis) and rinsed with PBS to allow for an approximately 2.4-fold

expansion of the sample followed by immediate confocal imaging. The diameters of the gelled coverslips were measured pre- and post-expansion with a ruler to calculate the expansion factor.

Brain sections

Brain sections were obtained as described above. Polymer solution (as described above) with additional 0.02% (w/w) 4-hydroxy tempo (Sigma) was added onto brain sections in gelling chamber, followed by 30 min incubation at 4 °C. In situ polymerization was then facilitated by a 2 h incubation step at 37 °C. Gelled brain sections were then further dissected for regions of interests and transferred into 1.5 mL microcentrifuge tubes containing 0.5 mL digestion solution (200 mM SDS, 200 mM NaCl, 50 mM Tris, pH 9). To allow for equidistant expansion, samples were incubated for 37 °C and 95 °C for 1 h, respectively. After digestion, samples were rinsed five times with PBS, followed by a 2 h incubation in blocking solution (% donkey serum, 0.1% Triton X-100 in PBS). Primary antibodies were diluted in 5% donkey serum in PBS and gelled samples were incubated for a minimum of 24 h at °C [52, 53]. The following antibodies were used: anti- $\alpha\beta$ synuclein (Abcam, RRID: AB_869971), anti-vGLUT1 (Synaptic Systems, RRID: AB_887878), anti-Homer1 (Synaptic Systems RRID: AB_2631222). ExM samples were incubated for 24 h in Alexa-Fluor conjugated secondary antibodies at 4 °C. The expansion factor was calculated by measuring the dorsal–ventral and medial–lateral distances in coronal mouse brain sections stained with Hoechst 33342 for pre- and post-expansion tissue.

Confocal microscopy and image analysis

Confocal imaging was performed on a Nikon A1R Confocal microscope with 40X and 60X oil immersion objectives. Primary neuron ExM samples in imaging plates were imaged with an inverted Nikon C2+ confocal with a galvanometer-based high-speed scanning and an apochromatic long working distance 40X water immersion objective. Brain sections were imaged as z-stacks (step size 0.2 μm) on a Nikon A1R Confocal microscope. For colocalization analysis, the coloc2 plugin for FIJI was used and the thresholded Mander's Colocalization Coefficient (MCC) calculated. For distance measurements for ExM primary neuron experiments, synapses were identified by juxtaposed pre- and postsynaptic markers. A line perpendicular to the synaptic cleft was drawn, the grey intensity profile of each marker was plotted and the relative peak fluorescence to peak distance was measured to assess the relative distance between markers of interest. For tissue ExM experiments, maximal projection images were generated using Fiji, and synapses identified

as described in [44]. After synapse identification, a line perpendicular to the synaptic cleft was drawn and the fluorescent profiles of the markers of interest used to calculate the relative distance. Experimenters conducting imaging and analysis were blinded to experimental conditions.

Synaptosome fractionation

Three months old C57BL/6 J mice received PF-360 chow or control chow for 8 days. Brains were homogenized in 2 mL of sucrose buffer (320 mM sucrose, 2 mM DDT, 1 mM EDTA, 1 mM EGTA, 4 mM HEPES-KOH, pH 7.4, with protease and phosphatase inhibitors) using a Teflon dounce on ice with 10 strokes. Differential centrifugation was used to fractionate brain homogenate as described [54]. In brief, the total homogenate was centrifuged for 10 min (min) at 1,000 *g*, the post-nuclear supernatant was centrifuged for 10 min at 9,200 *g*, the resulting pellet was resuspended in sucrose buffer followed by centrifugation at 10,200 *g*. The resulting pellet is the synaptosome fraction, P2. The supernatant was further centrifuged for 2 h at 167,000 *g* to fractionate the total soluble protein fraction (S3) and the microsomal pellet (P3) which was resuspended in 700 μL sucrose buffer and homogenized in a glass dounce with ten up-and-down strokes. The P2 pellet was resuspended in 5 mM HEPES-KOH (pH 7.4) supplemented with protease and phosphatase inhibitors, homogenized in with a glass dounce and centrifuged for 20 min at 21,130 *g*. The resulting synaptosomal, membrane-enriched pellet (LP1) was resuspended in sucrose buffer and the supernatant was centrifuged for 2 h at 200,000 *g*. Finally, the sedimented synaptic vesicle-enriched fraction (LP2) was resuspended sucrose buffer and homogenized with a glass dounce. All isolated fractions were snap-frozen in EtOH/dry ice slurry and stored at -80 °C until use.

Statistics

All statistical analyses were performed using Graph Pad software. Data were presented as mean and standard error of the mean unless indicated differently in the figure legends. Nested independent t-test analysis or nested one-way ANOVA with Tukey's posthoc analyses were performed. If data did not fit a normal distribution, the Mann–Whitney test was used. Statistical analyses are presented in Table 1.

Results

LRRK2 kinase inhibition increases colocalization of α -synuclein and the presynaptic marker vGLUT1 in primary hippocampal neurons

α -Synuclein is highly expressed in glutamatergic presynaptic terminals where it colocalizes with vGLUT1 [15,

Table 1 List of statistical tests and results for each figure

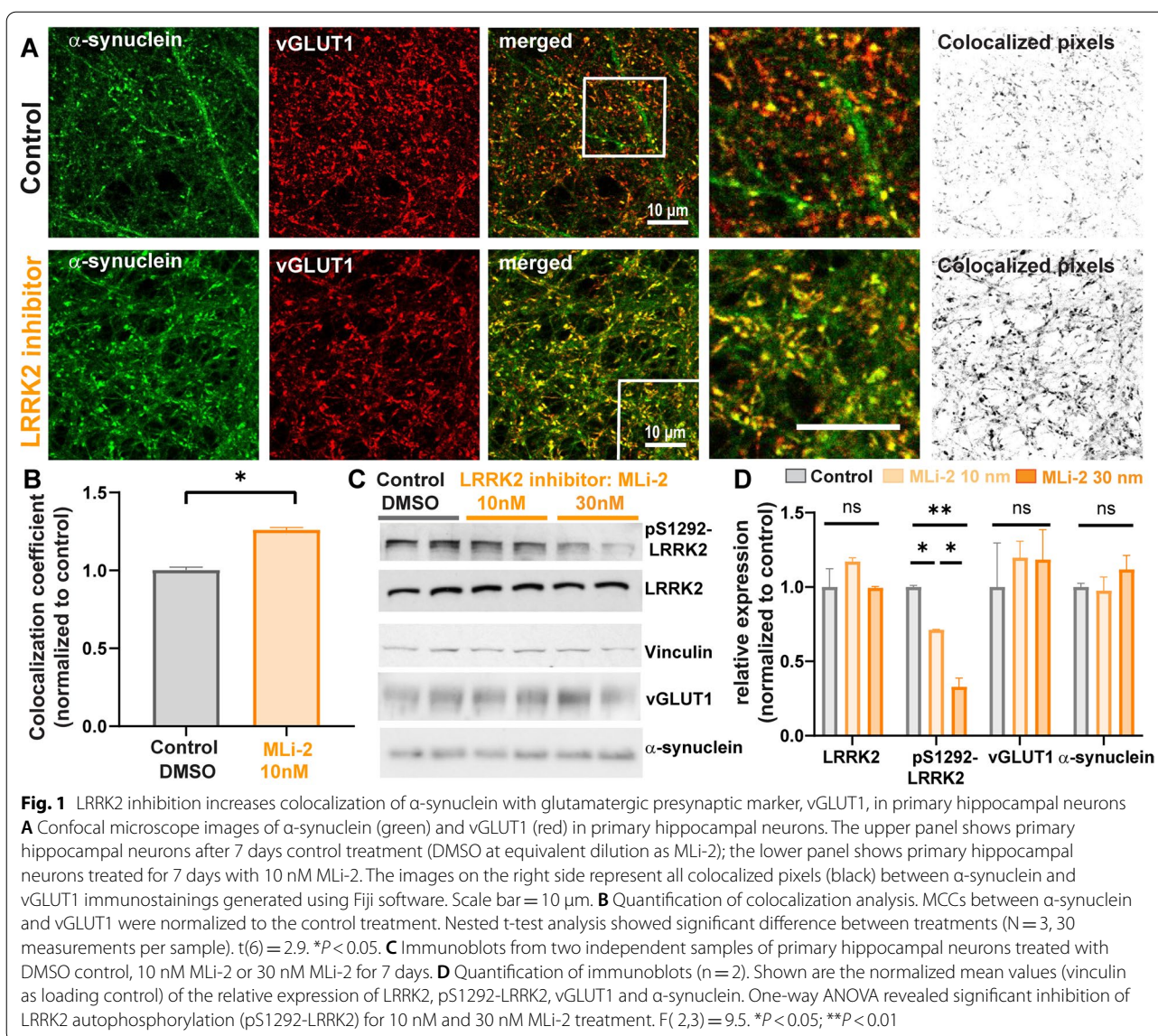
Figure	Graph identification	Type of test	Statistics
1B	vGLUT1/ α -synuclein	Nested t-test (two-tailed)	$t(6) = 2.9, P = 0.0284$
1D	LRRK2	One-way ANOVA	$F(2,3) = 1.9, P = 0.2896$
	pS1292-LRRK2	One-way ANOVA	$F(2,3) = 95.4, P = 0.0019$
	vGLUT1	One-way ANOVA	$F(2,3) = 0.3, P = 0.7839$
	α -synuclein	One-way ANOVA	$F(2,3) = 1.0, P = 0.4700$
2D	vGLUT1/Homer1	Nested t-test (two-tailed)	$t(2) = 0.8, P = 0.5135$
	vGLUT1/ α -synuclein	Nested t-test (two-tailed)	$t(116) = 6.5, P < 0.0001$
3B	Mobile tracks	Nested t-test (two-tailed)	$t(6) = 3.4, P = 0.0144$
	Vesicle count	Nested t-test (two-tailed)	$t(6) = 0.6, P = 0.5983$
	Anterograde tracks	Nested t-test (two-tailed)	$t(51) = 2.2, P = 0.0332$
	Retrograde tracks	Nested t-test (two-tailed)	$t(6) = 0.5, P = 0.6570$
3D	Anterograde tracks	Nested t-test (two-tailed)	$t(6) = 0.4, P = 0.7229$
	Retrograde tracks	Nested t-test (two-tailed)	$t(87) = 1.8, P = 0.0785$
4A	LRRK2	One-way ANOVA	$F(2,3) = 0.3, P = 0.76$
	pS935-LRRK2	One-way ANOVA	$F(2,3) = 54.35, P < 0.0001$
4B	LRRK2	Mann–Whitney test	$P = 0.800$
	pS1292	Mann–Whitney test	$P = 0.200$
	DAT	Mann–Whitney test	$P = 0.800$
	vGLUT1	Mann–Whitney test	$P = 0.400$
	α -synuclein	Mann–Whitney test	$P = 0.800$
4C	α -synuclein LP2	Independent t-test	$t(4) = 1.8, P = \text{NS}$
5C	vGLUT1/ α -synuclein	Nested t-test (two-tailed)	$t(6) = 3.3, P = 0.035$
5D	DAT/ α -synuclein	Nested t-test (two-tailed)	$t(178) = 6.6, P < 0.0001$
6D	vGLUT1/Homer1	Nested t-test (two-tailed)	$t(4) = 0.6, P = 0.5685$
	vGLUT1/ α -synuclein	Nested t-test (two-tailed)	$t(4) = 5.3, P = 0.0063$

55]. Furthermore, LRRK2 is also expressed in excitatory corticostriatal neurons [56], where its kinase activity influences striatal excitatory transmission [57–59]. To determine if LRRK2 kinase activity affects presynaptic localization of α -synuclein, primary hippocampal neurons, which are predominantly glutamatergic, were treated with the LRRK2 kinase inhibitor MLi-2, a selective LRRK2 kinase inhibitor [60], or DMSO vehicle control for 7 days [10]. Double labeling immunofluorescence and confocal microscopy were performed for α -synuclein and vGLUT1. In control primary hippocampal neurons, α -synuclein colocalized with vGLUT1 at excitatory presynaptic terminals (Fig. 1A). In neurons treated with MLi-2 for 7 days, colocalization of α -synuclein and vGLUT1 significantly increased compared to control neurons (Fig. 1A, B). Immunoblots of primary hippocampal neuron lysates treated with DMSO control or MLi-2 (10 nM, 30 nM) using an antibody that selectively recognizes the LRRK2 autophosphorylation site, S1292 [61], showed that MLi-2 significantly reduced LRRK2 kinase activity. Expression levels of α -synuclein and vGLUT1 were not significantly altered upon 7 days of LRRK2 kinase inhibition (Fig. 1C, D). In addition to

unaltered protein expression of the glutamatergic terminal marker vGLUT1 upon MLi-2 treatment, inhibition of LRRK2 kinase activity did not alter the overall density of glutamatergic terminals in primary hippocampal cultures (Additional file 1: Fig. S1). These findings suggest that LRRK2 kinase activity increases the localization of α -synuclein at the presynaptic terminal.

LRRK2 kinase inhibition increases α -synuclein overlap with presynaptic vGLUT1

LRRK2 localizes both pre- and post-synaptically in the rodent brain [56]. ExM was used to resolve the presynaptic terminal, postsynaptic densities, and localization of α -synuclein. ExM overcomes resolution limitations of traditional light microscopy by physically expanding the sample [51, 52, 62]. In traditional confocal images, α -synuclein colocalized with presynaptic vGLUT1, but both also showed overlap with the post-synaptic density marker, Homer1 (Fig. 2A). By using ExM, the resolution of confocal images was increased by 2.4 X, allowing presynaptic vGLUT1 and α -synuclein to be visibly distinguished from postsynaptic Homer1 (Fig. 2B). In primary hippocampal neurons treated with 10 nM MLi-2

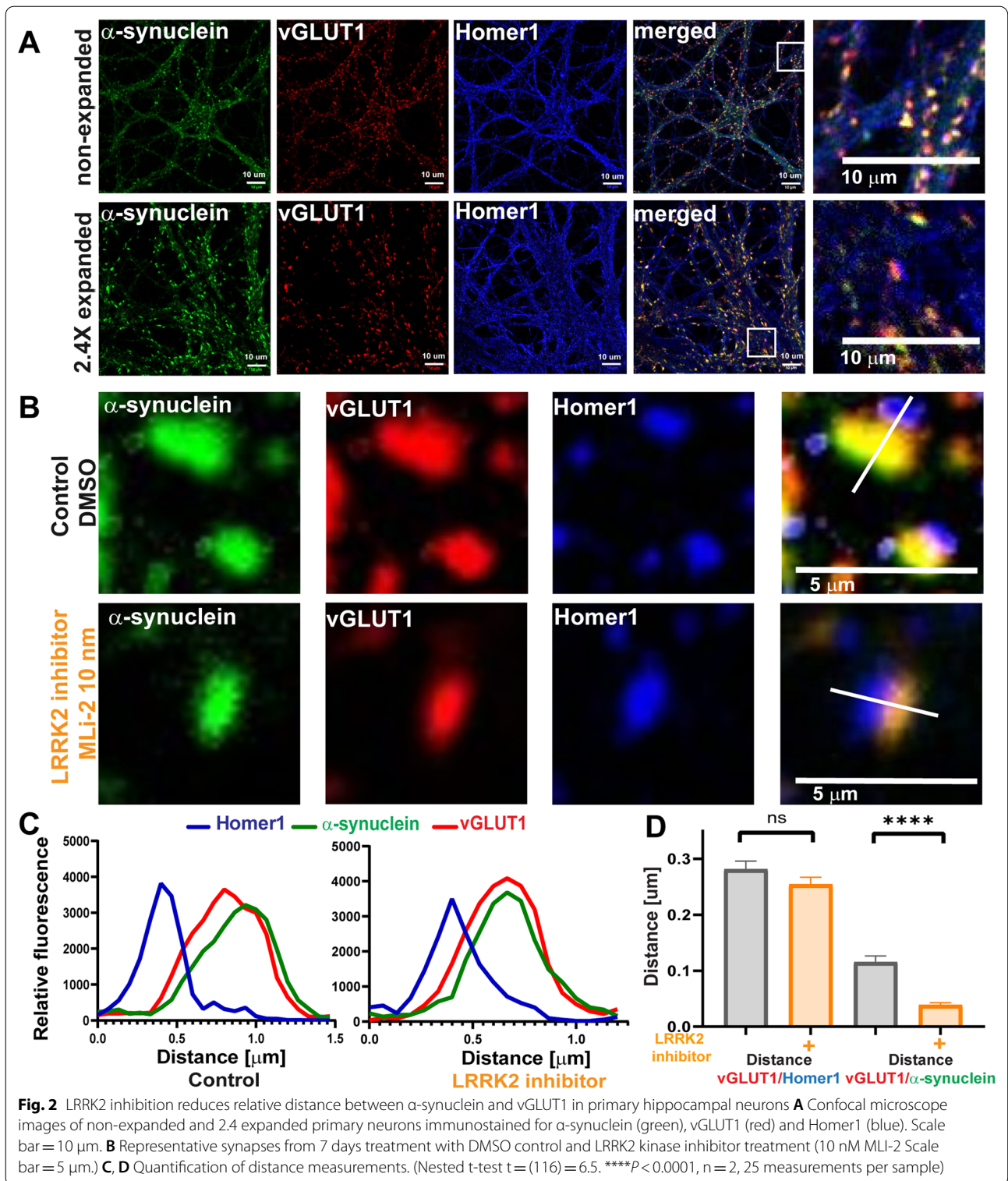


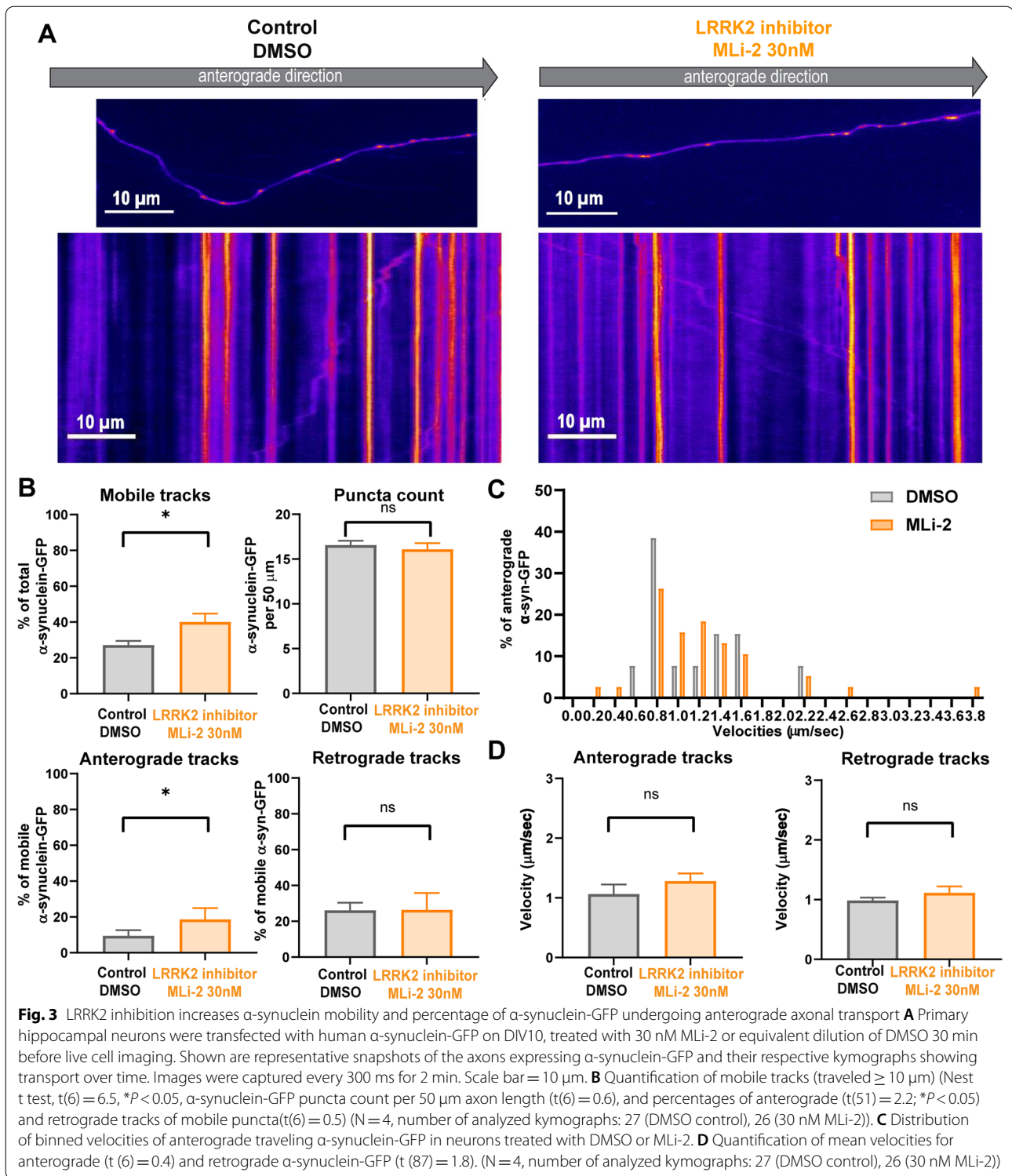
for 7 days, α -synuclein showed increased colocalization with vGLUT1 (Fig. 1C, D). The distance between the maximal fluorescence intensity peaks [44, 62] of Homer1 and vGLUT1 in control neurons was approximately 0.28 μ m and was not significantly altered in MLI-2 treated neurons compared to control treated neurons, indicating no change in the distance across the synaptic cleft (Fig. 2B–D). The distance between the maximal fluorescence intensity peaks of α -synuclein and vGLUT1 was significantly reduced in MLI-2 treated neurons (average of 0.04 μ m) compared to control neurons (average of 0.12 μ m), indicating increased overlap of α -synuclein and presynaptic vGLUT1 (Fig. 2B–D). These data demonstrate that increased overlap of α -synuclein with vGLUT1 at the presynaptic terminal is not a result of altered

pre- and postsynaptic morphology in general, rather a redistribution of α -synuclein caused by reduced LRRK2 kinase activity. In addition, these experiments confirm that unlike traditional confocal microscopy, ExM provides a method of quantifying changes in protein localizations in small, subcellular compartments.

LRRK2 kinase inhibition increased α -synuclein motility and anterograde trafficking

A portion of α -synuclein associates with membranes traveling via fast axonal transport in both anterograde and retrograde directions [48]. To determine if increased anterograde axonal transport at least partially accounts for enhanced localization of α -synuclein at the presynaptic terminal in response to LRRK2 kinase inhibition,





we transfected cells with α -synuclein-GFP and imaged axonal transport using live cell microscopy. Neurons were treated with 30 nM MLI-2 30 min prior to imaging. Figure 3A shows examples of axons containing

α -synuclein-GFP puncta and representative kymographs demonstrating puncta movement over time. Pharmacological reduction of LRRK2 kinase activity with MLI-2 treatment significantly increased the percentage

of mobile α -synuclein carriers moving in the anterograde direction, but did not impact the percentage of mobile carriers in the retrograde direction (Fig. 3B). Non-directional mobile puncta were classified by moving puncta that did not reach the net vectorial distance of 10 μm in either direction. The percentage of mobile α -synuclein-GFP was significantly increased (Fig. 3B). The overall abundance of α -synuclein puncta was unaltered. The overall net velocities of anterogradely traveling α -synuclein-GFP puncta were not significantly different between control and MLI-2 treated neurons (Fig. 3D). Analyses of binned velocities of α -synuclein-GFP particles (see [40]) revealed a shift toward faster velocities relative to the control neurons (Fig. 3C), however the differences in velocities between control and MLI-2 treated neurons were not significant. Overall, these data indicate that LRRK2 kinase inhibition increases movement of membranes bearing α -synuclein toward the presynaptic terminal.

LRRK2 and α -synuclein are enriched at presynaptic vesicle membranes in vivo

To determine if LRRK2 kinase inhibition affects α -synuclein localization in vivo, an in-diet dosing approach for chronic LRRK2 inhibition was used as described previously [46]. C57BL/6 J were fed chow formulated with 175 or 350 mg kg^{-1} PF-360 for 7 days to achieve chronic LRRK2 kinase inhibition. Reductions in LRRK2 kinase activity were assessed by immunoblotting for pS935-LRRK2 and total LRRK2 protein to determine the ratio of phospho-to-total LRRK2 in forebrain homogenates. pS935-LRRK2 levels are considered an indirect measure of LRRK2 kinase activity [46, 63, 64]. Both concentrations of PF-360 chow demonstrated reduced levels of pS935-LRRK2 without reducing total LRRK2 protein levels (Fig. 4A), as previously shown [46].

A separate cohort of mice fed either control or PF-360 chow (175 mg/kg) for 7 days was processed for whole brain lysates for immunoblot analyses of synaptic markers of interest for this study. In addition to synaptic marker and α -synuclein immunoblotting, the levels of the direct LRRK2 kinase phosphorylation site pS1292-LRRK2 were also assessed (Fig. 4B). While PF-360 treatment reduced levels of pS1292-LRRK2, quantification did not reveal a statistically significant change. Levels of presynaptic markers vGLUT1 and dopamine transporter (DAT) were not changed upon PF-360 treatment, nor did α -synuclein levels change upon LRRK2 kinase inhibitor treatment.

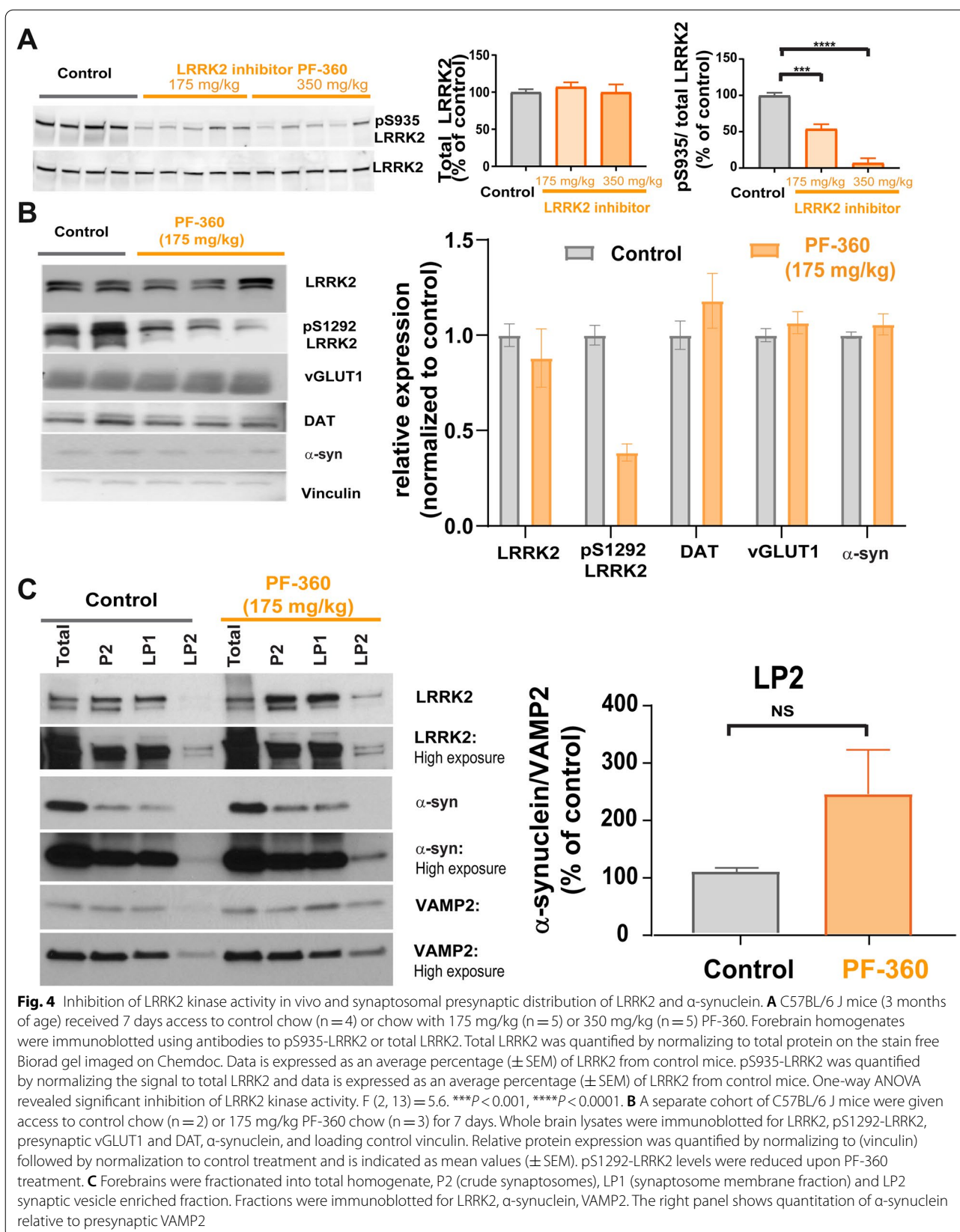
LRRK2 localizes to and plays a functional role at the presynaptic terminal [18, 20, 21, 23, 24, 65]. In addition, α -synuclein has been shown to be enriched at glutamatergic terminals [15, 55]. Synaptosome fractionation of

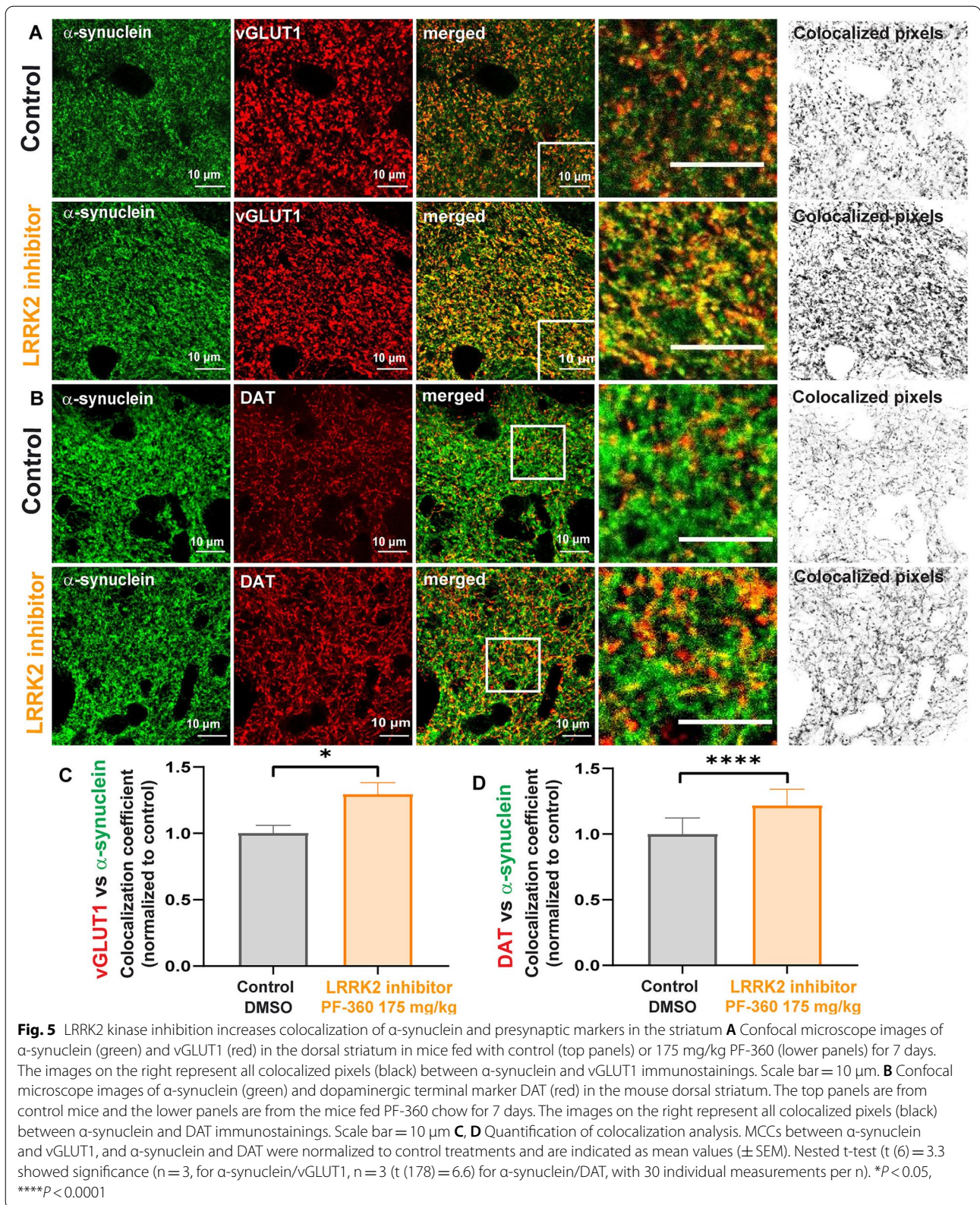
forebrain homogenates in a separate cohort of C57BL/6 J mice were used to determine whether 7 days of treatment with PF-360 altered localization of α -synuclein in the synaptic vesicle fraction. First, we found that LRRK2 localized to the synaptic vesicle enriched fraction LP2, confirming presynaptic LRRK2 (Fig. 4C). Immunofluorescence co-labelling for LRRK2 and presynaptic marker vGLUT1 and VAMP2 revealed colocalized puncta in the mouse brain striatum (Additional file 2: Fig. S2), further demonstrating LRRK2 localization glutamatergic presynaptic terminals. LRRK2 KO striatum showed minimal LRRK2 immunofluorescence signal (Additional file 2: Fig. S2), demonstrating specificity of our LRRK2 immunofluorescence results.

Seven days of treatment with PF-360 increased the proportion of α -synuclein in the LP2 fraction relative to controls, consistent with our imaging experiments in primary hippocampal neurons. These data show that LRRK2 and α -synuclein localize to the presynaptic terminal in the striatum in vivo.

LRRK2 kinase inhibition increases overlap of α -synuclein and presynaptic markers in the mouse striatum in vivo

To assess whether LRRK2 kinase inhibition increases presynaptic localization of α -synuclein in cortico-striatal and nigral-striatal presynaptic terminals, immunofluorescence and confocal microscopy for α -synuclein and vGLUT1, or DAT were performed in striatal sections from mice fed PF-360 (175 mg/kg) or control chow for 7 days (Fig. 6A). In control mice, the majority of α -synuclein overlapped with vGLUT1 as demonstrated previously [15]. Upon LRRK2 kinase inhibition, the overlap of α -synuclein with vGLUT1 significantly increased, similar to the findings in primary excitatory neurons. A smaller portion of α -synuclein colocalized with DAT (Fig. 5B). LRRK2 kinase inhibitor treatment increased colocalization of α -synuclein and DAT. Thus, LRRK2 kinase inhibition also increases α -synuclein presynaptic localization in the striatum in vivo. Immunoblotting analysis for whole brain lysates of rodents fed PF-360 showed that LRRK2 kinase inhibition did not change the overall protein expression levels of α -synuclein, vGLUT1, or DAT (Fig. 4B). In addition, LRRK2 kinase inhibition did not alter the density of glutamatergic terminals in the mouse brain striatum of animals fed PF-360 compared to control chow animals (Additional file 1: Fig. S1). The integrated density of DAT signal in the dorsal mouse striatum was significantly increased upon LRRK2 kinase inhibition compared to control animals (Additional file 1: Fig. S1). To increase the resolution of α -synuclein, vGLUT1, and Homer1 in the striatum, we performed ExM of striatal mouse brain sections and analyzed individual synapses for the subcellular localization of α -synuclein relative to





the presynaptic marker. ExM allowed resolution of synaptic markers in the mouse brain striatum compared to non-expanded samples (Fig. 6A). The results of individual synapse analyses utilizing ExM revealed a significantly reduced overall distance between α -synuclein and vGLUT1 at the presynaptic terminal of glutamatergic neurons projecting into the mouse striatum for animals treated with PF-360 (Fig. 6C, D). In addition, no change in the distance between Homer1 and vGLUT1 was observed upon LRRK2 kinase inhibition, and thus morphological synaptic structural rearrangements do not account for the reduced distance between α -synuclein and vGLUT1. No effect of LRRK2 kinase inhibition on the localization of the presynaptic protein synapsin-1 at glutamatergic terminals in the striatum was observed (Additional file 3: Fig. S3). Overall, our data demonstrate in primary neurons in culture and in mouse brains in vivo that reduced LRRK2 kinase activity increases presynaptic targeting of α -synuclein.

Discussion

The data in this study reveal that inhibition of LRRK2 kinase activity alters the axonal transport and presynaptic localization of α -synuclein in neurons. ExM provided a method to expand the tissue to more precisely resolve and quantify proximity between α -synuclein and synaptic markers. Inhibition of LRRK2 kinase activity in both primary neurons in vitro and in mouse striatum in vivo significantly increased colocalization of α -synuclein with presynaptic markers. Reduced LRRK2 kinase activity increased localization of α -synuclein with presynaptic vGLUT1 in excitatory terminals, and overlap of α -synuclein and DAT in dopamine axons. Lastly, LRRK2 kinase inhibition also increased the motility and anterograde transport of α -synuclein in axons. We previously demonstrated that neuronal expression of G2019S-LRRK2 with elevated kinase activity increases the cytosolic fraction of α -synuclein, and multiple studies show G2019S-LRRK2 increases the abundance of pathologic α -synuclein inclusions [6–11, 17, 66]. Thus, together, these data suggest that LRRK2 kinase activity may influence the ability of α -synuclein to form pathologic aggregates by controlling the presynaptic targeting of α -synuclein.

There are several mechanisms by which LRRK2 may convert normal α -synuclein to a conformation that

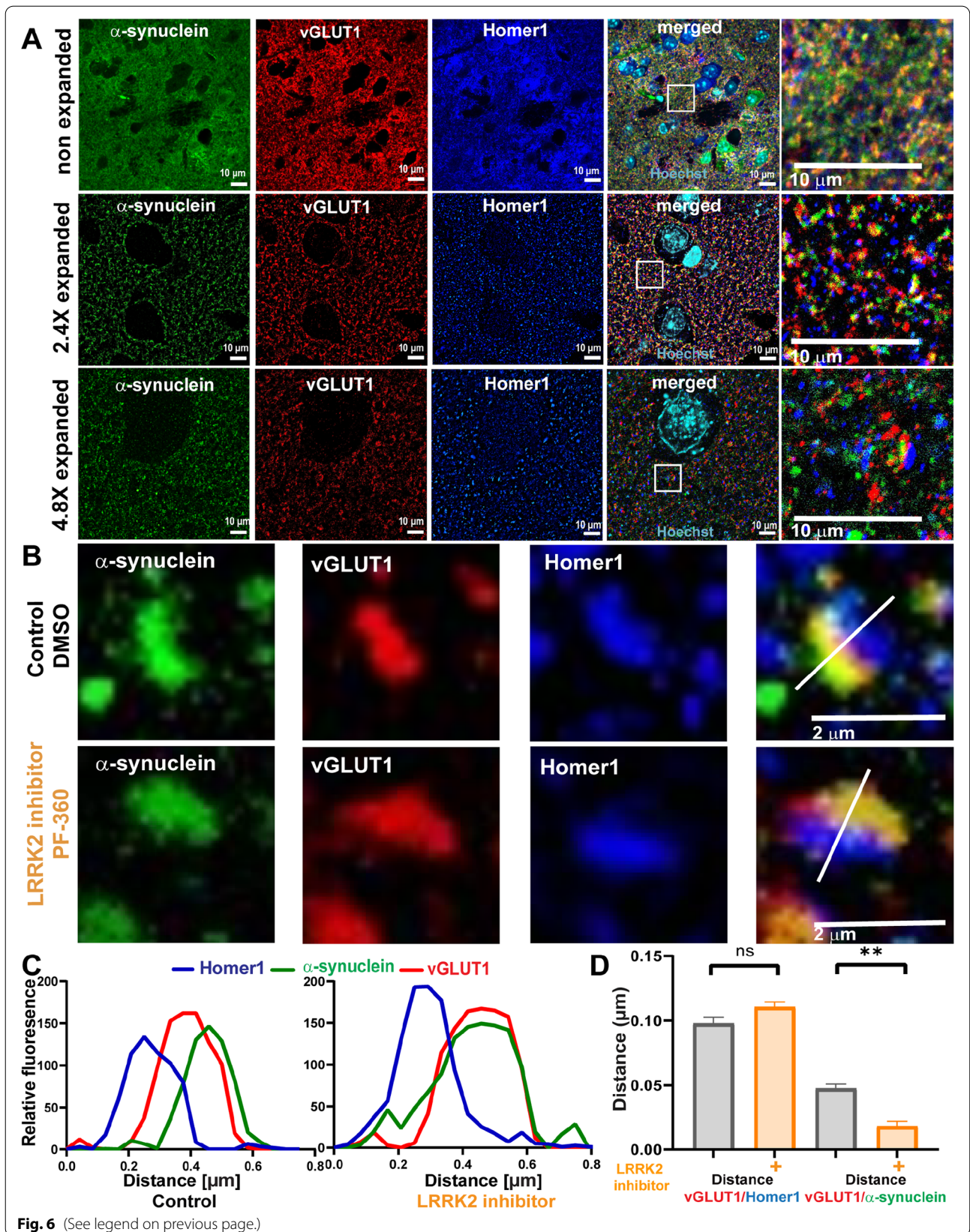
forms pathologic fibrils, including impairment of chaperone-mediated autophagy, or increased synthesis [67, 68]. LRRK2 also plays a major role in membrane trafficking [25, 69]. Defects in trafficking and targeting of α -synuclein to the correct membrane compartment within the neuron may influence its propensity to aggregate [70]. α -Synuclein primarily localizes to the presynaptic terminal [16, 71–74] where it interacts with the SNARE complex to reduce synaptic vesicle exocytosis [13, 14]. α -Synuclein preferentially associates with synaptic vesicle membranes and lipids as multimers, which protect the protein from forming β -sheets, and eventually inclusions [29–32]. We previously showed using fluorescence recovery after photobleaching that expression of G2019S-LRRK2 increases the cytosolic fraction of α -synuclein [10]. The current study demonstrated that inhibition of LRRK2 kinase activity increases the normal localization of α -synuclein at the presynaptic terminal. Therefore, in addition to LRRK2-mediated alterations in proteostasis, the effect of LRRK2 on α -synuclein subcellular localization may be another mechanism by which it influences formation of pathologic inclusions.

LRRK2 and α -synuclein are highly expressed in excitatory neurons, [56]. LRRK2 kinase activity influences the physiological activity of excitatory neurons [56, 59, 75, 76]. High expression levels and the presynaptic enrichment of α -synuclein at glutamatergic terminals may have crucial implications for glutamate transmission [77, 78]. The interaction of α -synuclein and VAMP2 at excitatory terminals is thought to act as a break on vesicle release [79]. Because mutant LRRK2 increases corticostriatal excitatory transmission [58, 59] increased targeting of α -synuclein to the presynaptic terminal by LRRK2 kinase inhibitors may help dampen and rescue this aberrant activity [47]. Also, dopaminergic neurons are of major importance due to their selective vulnerability in PD. We showed that inhibition of LRRK2 kinase increases the overlap of α -synuclein and DAT in vivo, and observed an increase of DAT signal in the striatum of LRRK2 kinase inhibitor treated animals. Future experiments should elucidate the functional interaction of LRRK2 and α -synuclein in dopaminergic neurons.

To further elaborate, our data shows that inhibition of LRRK2 kinase activity increases localization of α -synuclein at the presynaptic terminal in vitro and in vivo. Our ExM data showed reduced proximity

(See figure on next page.)

Fig. 6 LRRK2 inhibition reduces relative distance between α -synuclein and vGLUT1 in the mouse striatum **A** Confocal microscope images of the striatum in non-expanded, 2.4x, and 4.8 x expanded brain sections immunostained for α -synuclein (green), vGLUT1 (red) and Homer1 (blue). Scale bar = 10 μ m. **B** Representative synapses upon control and LRRK2 kinase inhibitor treatment (7 days, 10 nM MLI-2). Scale bar = 2 μ m. **C** Respective fluorescent profiles from **B**. **D** Quantification of distance measurements in mean distance (\pm SEM) between Homer1 and vGLUT1 ($t(4) = 0.6$) and between vGLUT1 and α -synuclein ($t(4) = 5.3$ (nested t-test analysis, $n = 3$, 25 measurements per n). $**P < 0.01$



between α -synuclein and vGLUT1 at the presynaptic terminal upon LRRK2 kinase inhibition. Although the functional implications of increased targeting of α -synuclein to the presynaptic terminal are unknown, because α -synuclein can act as a brake on synaptic vesicle exocytosis it is possible that increased synaptic vesicle association of α -synuclein could reduce excitatory transmission [74, 78, 80, 81]. Previous studies using electrophysiological recordings in the striatum showed that increased LRRK2 kinase activity increases spontaneous evoked postsynaptic current frequency, suggesting increased cortico-striatal presynaptic activity. The increased cortico-striatal presynaptic activity is reversed by LRRK2 inhibition [20, 59, 65]. Cortico-striatal glutamatergic transmission and activity has been associated as a putative somatotopic stressor of dopaminergic neurons [82]. Thus, it is possible that mutant LRRK2 through its presynaptic actions on α -synuclein localization and glutamatergic synapse activity could cause a degeneration in dopamine terminals in the striatum, ultimately leading to Parkinson's disease. Although LRRK2 inhibition did not affect localization of synapsin-1, future studies should also investigate if the observed impact of LRRK2 kinase inhibition is specific for α -synuclein, or if other synaptic proteins might be affected [83]. Electron microscopy studies show that reduced levels of LRRK2 decreased the number of docked vesicles at the active zone, suggesting reduced LRRK2 activity could impact synaptic proteins involved in docking [84].

We also found that LRRK2 kinase inhibition increases α -synuclein colocalization with DAT in the dorsal striatum. A synergistic interaction of DAT and α -synuclein has been previously reported, as DAT activity is thought to increase membrane association of α -synuclein which in turn targets DAT to cholesterol-rich membrane domains [85]. Pathological LRRK2 mutations have been shown to reduce dopamine transporters in the striatum for patients with and without a PD diagnosis [86]. Our data showed increased DAT signal in the dorsal striatum of animals treated with LRRK2 kinase inhibitor, while overall expression of DAT was unaltered, indicating re-localization or trafficking of DAT. DAT has also been shown to mislocalize in PD post mortem brain tissue, where close proximity of DAT to aggregate-like α -synuclein has been reported [87]. Thus, the data in this study point toward a possible critical link between LRRK2 kinase activity and α -synuclein in regulating DAT activity and trafficking. Further experiments will be needed to investigate the spatial relationships and functional interactions of LRRK2, α -synuclein, and DAT.

Our data suggest that LRRK2 kinase inhibition increases α -synuclein axonal transport toward the presynaptic terminal. Although slow component B, a

transport mechanism mediating axonal trafficking of soluble proteins, is thought to be the primary driver of cytosolic α -synuclein transport [88], fast axonal transport of α -synuclein on vesicles also occurs [48]. In our control neurons, there were few α -synuclein particles traveling via fast axonal transport, but this significantly increased upon LRRK2 kinase inhibition. Additionally, overall motility of α -synuclein-GFP puncta was significantly increased upon LRRK2 kinase inhibitor treatment. LRRK2 kinase inhibition significantly decreased the percentage of immobile puncta. Our data contribute to multiple emerging studies demonstrating a functional role for LRRK2 in microtubule-based axonal transport [26–28, 89]. Expression of the R1441C-LRRK2 or Y1699C-LRRK2 mutants inhibit axonal transport of mitochondria, which can be rescued by increasing microtubule acetylation [28]. The active conformation of LRRK2 associates with microtubules and blocks movement of kinesin and dynein motors [90]. Impaired balance of the kinesin and dynein motors by overactive LRRK2 reduces the processivity of autophagosome transport along the axon. Rab3a, an LRRK2 kinase substrate, mediates the interaction with kinesin-3 [91]; the active conformation of Rab3a promotes its interaction and consequently, overall anterograde trafficking of synaptic vesicle precursors in the axon. Importantly, LRRK2 kinase mediated phosphorylation of Rab GTPases is thought to disrupt their interactions with effectors [92–95]. In this way, it is conceivable that increased LRRK2 kinase activity might disrupt the transport mechanisms involving vesicles, Rabs, and associated motor proteins. Conversely, by inhibiting LRRK2 kinase activity, vesicle interactions and anterograde trafficking are promoted.

This study sheds light on the different roles LRRK2 might play in α -synuclein trafficking. These findings are consistent with previous studies demonstrating a major role of LRRK2 in membrane trafficking, and in axonal transport. Understanding LRRK2 kinase activity could be potentially important for putative treatment options of both LRRK2-PD and sporadic PD cases [4]. Given that tetrameric, native α -synuclein is resistant to aggregation [30, 38, 39], our data also suggest that LRRK2 kinase inhibitors could have a therapeutic benefit in halting Parkinson's disease progression and development of nonmotor symptoms by increasing native, presynaptic α -synuclein at membranes and protecting against pathologic aggregation.

Conclusions

Both LRRK2 and α -synuclein localize to the presynaptic terminal, and LRRK2 kinase activity has been shown by multiple studies to impact pathologic α -synuclein aggregation, but how LRRK2 kinase influences normal

α -synuclein has remained unclear. This study shows that inhibition of LRRK2 kinase activity increases presynaptic targeting of α -synuclein. Treatment with the selective LRRK2 inhibitors MLI-2 and PF-360 in primary neurons *in vitro* and in the mouse striatum *in vivo* increased overlap of α -synuclein and glutamatergic terminal marker, vGLUT1. In addition, using the high resolution imaging technique expansion microscopy to resolve and quantify changes in α -synuclein presynaptic localization, we show that inhibition of LRRK2 kinase increases the overlap of α -synuclein and vGLUT1. Live cell imaging experiments showed increased motility and anterograde trafficking of α -synuclein-GFP puncta upon LRRK2 kinase activity, consistent with growing evidence for a role of LRRK2 in axonal transport. Overall, this study demonstrate a role of LRRK2 kinase activity in α -synuclein localization at the presynaptic terminal which suggest a role for these two proteins in synaptic dysfunction and PD-related phenotypes.

Abbreviations

DAT: Dopamine transporter; ExM: Expansion microscopy; LRRK2: Leucine-rich repeat kinase 2; MCC: Mander's Colocalization coefficient; PD: Parkinson's disease; VAMP2: Vesicle-associated membrane protein 2; vGLUT1: Vesicular glutamate transporter 1.

Supplementary Information

The online version contains supplementary material available at <https://doi.org/10.1186/s40478-021-01283-7>.

Additional file 1: Fig. S1. No change in glutamatergic terminal density upon LRRK2 kinase inhibitor treatment. A) Shown are confocal images of primary hippocampal neurons stained for vGLUT1 (red), the above-threshold signal (black) and counted particles (bright blue) per frame. The obtained data is quantified in the graph of the right. No change in glutamatergic terminal density was observed for LRRK2 kinase inhibitor treatment. (Nested t-test; $t = (58) = 1.16$, $p = 0.25$, $n=3$, 10 measurements per sample) B) Confocal images of glutamatergic terminals in coronal sections of the mouse striatum, the above-threshold signal (black) and counted particles (bright blue). No change of glutamatergic terminal density was observed upon LRRK2 kinase inhibitor treatment (PF-360). (Nested t-test; $t = (58) = 0.88$, $p = 0.38$, $n=3$, 10 measurements per sample) C) Shows are confocal images of the dorsal mouse striatum stained for DAT (red) and the above threshold signal (black) for control (left) and PF-360 treated animals (right). LRRK2 kinase inhibitor treatment significantly increased the integrated density of DAT signal compared to control, as visualized in the graph on the right. (Nested t-test; $t = (4) = 2.99$, $p = 0.04$, $*p < 0.05$, $n = 3$, 10 measurements per sample).

Additional file 2: Fig. S2. Reduction of LRRK2 immunofluorescence signal in LRRK2 KO mice. A) LRRK2 immunofluorescence in C57BL/6J LRRK2 KO mice (kindly provided by Dr. Matthew Goldberg, UAB) is visibly reduced in the striatum and cortex compared to wildtype mice. B) Confocal images of mouse brain sections immunostained for LRRK2 (green) and presynaptic markers (vGLUT1 in red, VAMP2 in blue) show colocalization, especially for glutamatergic terminals in the striatum.

Additional file 3: Fig. S3. No change of localization of synapsin-1 upon LRRK2 kinase inhibitor treatment. A) Colocalization analysis of a mouse cohort treated with LRRK2 kinase inhibitor PF-360 and control mice showed no significant difference in overlap of vGLUT1 (red) and Synapsin-1 (green). Confocal images of the dorsal striatum as well as colocalized pixel maps are shown for visualization. (Nested t-test $t = (2) = 0.43$, $p = 0.71$, $n = 2$, 9 measurements per sample).

B) High resolution imaging analysis with ExPath (Expansion Pathology, protocol adapted from Bucur et al. (2020), Nature Protocols) showed no significant change of synapsin-1 (blue) localization at the presynaptic terminal between control animals and PF-360 treated animals. Shown are confocal images of ExPath samples stained for presynaptic markers vGLUT1 (red) and Synapsin-1 (blue) and postsynaptic marker Homer1 (green). (Nested t-test: vGLUT1/Homer1: $t = (2) = 0.74$, $p = 0.54$, vGLUT1/synapsin-1: $t = (2) = 1.05$, $p = 0.40$, $n = 2$, 10 measurements per sample).

Acknowledgements

We also thank the staff of the UAB HRIF, particularly Dr. Alexa Mattheyses for the support and valuable input during high resolution imaging.

Authors' contributions

CFB and LVD designed experiments and overall hypothesis. LVD, CFB, BH, VS, NZG, KK and DS conducted experiments and the analysis, LVD and CFB interpreted the results. DS and ED provided ExM protocols and training. KK and AW provided PF-360 chow. LVD, CFB, BH and VS wrote the manuscript, NZG, KK, AW, DS and EB revised the manuscript. All authors read and approved the final manuscript.

Funding

This work is supported by National Institutes of Health (NIH) National Institute of Neurological Disorders and Stroke (NINDS) grants R01NS102257 and R56NS117465 (to L.A.V.-D.), Michael J Fox Foundation grant MJFF-004413 (to E.B. and L.A.V.-D.), and E.S.B. funding from Lisa Yang, John Doerr, Open Philanthropy, NIH 1R01EB024261, NIH R56NS117465, and Howard Hughes Medical Institute.

Availability of data and materials

The datasets used and/or analyzed during the current study are available from the corresponding author on reasonable request.

Declarations

Ethics approval and consent to participate

All animal protocols were approved by the Institutional Animal Care and Use Committee at the University of Alabama at Birmingham.

Consent for publication

All authors read and approved the final manuscript for publication.

Competing interests

The authors have no conflicts of interest to declare.

Author details

¹Department of Neurology, Center for Neurodegeneration and Experimental Therapeutics, University of Alabama at Birmingham, Birmingham, AL 35294, USA. ²Interfaculty Institute for Biochemistry, University of Tübingen, 72076 Tübingen, Germany. ³Duke Center for Neurodegeneration Research, Department of Pharmacology and Cancer Biology, Duke University, Durham, NC, USA. ⁴McGovern Institute for Brain Research, Massachusetts Institute of Technology, Cambridge, MA 02139, USA. ⁵Department of Brain and Cognitive Sciences, Massachusetts Institute of Technology, Cambridge, MA 02139, USA. ⁶Howard Hughes Medical Institute, Massachusetts Institute of Technology, Cambridge, MA 02139, USA. ⁷MIT Media Lab, Departments of Biological Engineering and Brain and Cognitive Sciences, Massachusetts Institute of Technology, Cambridge, MA 02139, USA.

Received: 12 August 2021 Accepted: 20 October 2021

Published online: 08 November 2021

References

- Spillantini MG, Schmidt ML, Lee VM, Trojanowski JQ, Jakes R, Goedert M (1997) Alpha-synuclein in Lewy bodies. *Nature* 388(6645):839–840

2. Paisan-Ruiz C, Jain S, Evans EW, Gilks WP, Simon J, van der Brug M, de Lopez MA, Aparicio S, Gil AM, Khan N et al (2004) Cloning of the gene containing mutations that cause PARK8-linked Parkinson's disease. *Neuron* 44(4):595–600
3. Zimprich A, Biskup S, Leitner P, Lichtner P, Farrer M, Lincoln S, Kachergus J, Hulihan M, Uitti RJ, Calne DB et al (2004) Mutations in LRRK2 cause autosomal-dominant parkinsonism with pleomorphic pathology. *Neuron* 44(4):601–607
4. Di Maio R, Hoffman EK, Rocha EM, Keeney MT, Sanders LH, De Miranda BR, Zharikov A, Van Laar A, Stepan AF, Lanz TA et al (2018) LRRK2 activation in idiopathic Parkinson's disease. *Science translational medicine* 10(451):67
5. Kalia LV, Lang AE, Hazrati LN, Fujioaka S, Wszolek ZK, Dickson DW, Ross OA, Van Deerlin VM, Trojanowski JQ, Hurtig HI et al (2015) Clinical correlations with Lewy body pathology in LRRK2-related Parkinson disease. *JAMA Neurol* 72(1):100–105
6. Bae EJ, Kim DK, Kim C, Mante M, Adame A, Rockenstein E, Ulusoy A, Klinkenberg M, Jeong GR, Bae JR et al (2018) LRRK2 kinase regulates alpha-synuclein propagation via RAB35 phosphorylation. *Nat Commun* 9(11):3465
7. Bieri G, Brahm C, Bousset L, Couthouis J, Kramer NJ, Ma R, Nakayama L, Monbureau M, Defensor E, Schule B et al (2019) LRRK2 modifies alpha-syn pathology and spread in mouse models and human neurons. *Acta Neuropathol* 137(6):961–980
8. Lin X, Parisiadou L, Gu XL, Wang L, Shim H, Sun L, Xie C, Long CX, Yang WJ, Ding J et al (2009) Leucine-rich repeat kinase 2 regulates the progression of neuropathology induced by Parkinson's-disease-related mutant alpha-synuclein. *Neuron* 64(6):807–827
9. Schapansky J, Khasnavis S, DeAndrade MP, Nardozi JD, Falkson SR, Boyd JD, Sanderson JB, Bartels T, Melrose HL, LaVoie MJ (2018) Familial knockin mutation of LRRK2 causes lysosomal dysfunction and accumulation of endogenous insoluble alpha-synuclein in neurons. *Neurobiol Dis* 111:26–35
10. Volpicelli-Daley LA, Abdelmotilib H, Liu Z, Stoyka L, Daher JP, Milnerwood AJ, Unni VK, Hirst WD, Yue Z, Zhao HT et al (2016) G2019S-LRRK2 expression augments alpha-synuclein sequestration into inclusions in neurons. *J Neurosci Off J Soc Neurosci* 36(28):7415–7427
11. Zhao HT, John N, Delic V, Ikeda-Lee K, Kim A, Weihofen A, Swayze EE, Kordasiewicz HB, West AB, Volpicelli-Daley LA (2017) LRRK2 antisense oligonucleotides ameliorate alpha-synuclein inclusion formation in a parkinson's disease mouse model. *Mol Ther Nucleic Acids* 8:508–519
12. Atias M, Tevet Y, Sun J, Stavsky A, Tal S, Kahn J, Roy S, Gitler D (2019) Synapsins regulate alpha-synuclein functions. *Proc Natl Acad Sci USA* 116(23):11116–11118
13. Burre J, Sharma M, Tsetsenis T, Buchman V, Etherton MR, Sudhof TC (2010) Alpha-synuclein promotes SNARE-complex assembly in vivo and in vitro. *Science (New York, NY)* 329(5999):1663–1667
14. Sun J, Wang L, Bao H, Premi S, Das U, Chapman ER, Roy S (2019) Functional cooperation of alpha-synuclein and VAMP2 in synaptic vesicle recycling. *Proc Natl Acad Sci USA* 116(23):11113–11115
15. Taguchi K, Watanabe Y, Tsujimura A, Tanaka M (2016) Brain region-dependent differential expression of alpha-synuclein. *J Comp Neurol* 524(6):1236–1258
16. Vargas KJ, Schrod N, Davis T, Fernandez-Busnadiego R, Taguchi YV, Laugks U, Lucic V, Chandra SS (2017) Synucleins have multiple effects on presynaptic architecture. *Cell Rep* 18(1):161–173
17. Ysselstein D, Joshi M, Mishra V, Griggs AM, Asiago JM, McCabe GP, Stanciu LA, Post CB, Rochet JC (2015) Effects of impaired membrane interactions on alpha-synuclein aggregation and neurotoxicity. *Neurobiol Dis* 79:150–163
18. Arranz AM, Delbroek L, Van Kolen K, Guimaraes MR, Mandemakers W, Daneels G, Matta S, Calafate S, Shaban H, Baatsen P et al (2015) LRRK2 functions in synaptic vesicle endocytosis through a kinase-dependent mechanism. *J Cell Sci* 128(3):541–552
19. Cirnaru MD, Marte A, Belluzzi E, Russo I, Gabrielli M, Longo F, Arcuri L, Murre L, Bubacco L, Matteoli M et al (2014) LRRK2 kinase activity regulates synaptic vesicle trafficking and neurotransmitter release through modulation of LRRK2 macro-molecular complex. *Front Mol Neurosci* 7:49
20. Matikainen-Ankney BA, Kezunovic N, Menard C, Flanigan ME, Zhong Y, Russo SJ, Benson DL, Huntley GW (2018) Parkinson's disease-linked LRRK2-G2019S mutation alters synaptic plasticity and promotes resilience to chronic social stress in young adulthood. *J Neurosci Off J Soc Neurosci* 38(45):9700–9711
21. Pan PY, Zhu Y, Shen Y, Yue Z (2019) Crosstalk between presynaptic trafficking and autophagy in Parkinson's disease. *Neurobiol Dis* 122:64–71
22. Hu D, Niu JY, Xiong J, Nie SK, Zeng F, Zhang ZH (2018) LRRK2 G2019S mutation inhibits degradation of alpha-synuclein in an in vitro model of Parkinson's disease. *Curr Med Sci* 38(6):1012–1017
23. Pischedda F, Piccoli G (2021) LRRK2 at the pre-synaptic site: a 16-years perspective. *J Neurochem* 157(2):297–311
24. Matta S, Van Kolen K, da Cunha R, van den Bogaart G, Mandemakers W, Miskiewicz K, De Bock PJ, Morais VA, Vilain S, Haddad D et al (2012) LRRK2 controls an EndoA phosphorylation cycle in synaptic endocytosis. *Neuron* 75(6):1008–1021
25. Cookson MR (2016) Cellular functions of LRRK2 implicate vesicular trafficking pathways in Parkinson's disease. *Biochem Soc Trans* 44(6):1603–1610
26. Boecker CA, Holzbaur ELF (2021) Hyperactive LRRK2 kinase impairs the trafficking of axonal autophagosomes. *Autophagy* 2:1–3
27. Boecker CA, Goldsmith J, Dou D, Cajka GG, Holzbaur ELF (2021) Increased LRRK2 kinase activity alters neuronal autophagy by disrupting the axonal transport of autophagosomes. *Current biology : CB* 31(10):2140–2154. e2146
28. Godena VK, Brookes-Hocking N, Moller A, Shaw G, Oswald M, Sancho RM, Miller CC, Whitworth AJ, De Vos KJ (2014) Increasing microtubule acetylation rescues axonal transport and locomotor deficits caused by LRRK2 Roc-COR domain mutations. *Nat Commun* 5:5245
29. Burre J, Sharma M, Sudhof TC (2015) Definition of a molecular pathway mediating alpha-synuclein neurotoxicity. *J Neurosci Off J Soc Neurosci* 35(13):5221–5232
30. Burre J, Sharma M, Sudhof TC (2014) alpha-Synuclein assembles into higher-order multimers upon membrane binding to promote SNARE complex formation. *Proc Natl Acad Sci USA* 111(40):E4274–4283
31. Dettmer U, Newman AJ, Soldner F, Luth ES, Kim NC, von Saucken VE, Sanderson JB, Jaenisch R, Bartels T, Selkoe D (2015) Parkinson-causing alpha-synuclein missense mutations shift native tetramers to monomers as a mechanism for disease initiation. *Nat Commun* 6:7314
32. Dettmer U, Newman AJ, von Saucken VE, Bartels T, Selkoe D (2015) KTKEGV repeat motifs are key mediators of normal alpha-synuclein tetramerization: their mutation causes excess monomers and neurotoxicity. *Proc Natl Acad Sci USA* 112(31):9596–9601
33. Fusco G, De Simone A, Arosio P, Vendruscolo M, Veglia G, Dobson CM (2016) Structural ensembles of membrane-bound alpha-synuclein reveal the molecular determinants of synaptic vesicle affinity. *Sci Rep* 6:27125
34. Fusco G, De Simone A, Gopinath T, Vostrikov V, Vendruscolo M, Dobson CM, Veglia G (2014) Direct observation of the three regions in alpha-synuclein that determine its membrane-bound behaviour. *Nat Commun* 5:3827
35. Fonseca-Ornelas L, Eisbach SE, Paulat M, Giller K, Fernandez CO, Outeiro TF, Becker S, Zweckstetter M (2014) Small molecule-mediated stabilization of vesicle-associated helical alpha-synuclein inhibits pathogenic misfolding and aggregation. *Nat Commun* 5:5857
36. Burre J, Sharma M, Sudhof TC (2012) Systematic mutagenesis of alpha-synuclein reveals distinct sequence requirements for physiological and pathological activities. *J Neurosci Off J Soc Neurosci* 32(43):15227–15242
37. Fanning S, Haque A, Imberdis T, Baru V, Barrasa MI, Nuber S, Termine D, Ramalingam N, Ho GPH, Noble T et al (2019) Lipidomic analysis of alpha-synuclein neurotoxicity identifies stearyl CoA desaturase as a target for Parkinson treatment. *Mol Cell* 73(5):1001–1014
38. Dettmer U, Newman AJ, von Saucken VE, Bartels T, Selkoe D (2015) KTKEGV repeat motifs are key mediators of normal alpha-synuclein tetramerization: their mutation causes excess monomers and neurotoxicity. *Proc Natl Acad Sci USA* 112(31):9596–9601
39. Dettmer U, Newman AJ, Soldner F, Luth ES, Kim NC, von Saucken VE, Sanderson JB, Jaenisch R, Bartels T, Selkoe D (2015) Parkinson-causing alpha-synuclein missense mutations shift native tetramers to monomers as a mechanism for disease initiation. *Nat Commun* 6:7314
40. Volpicelli-Daley LA, Gamble KL, Schultheiss CE, Riddle DM, West AB, Lee VM (2014) Formation of alpha-synuclein Lewy neurite-like aggregates in axons impedes the transport of distinct endosomes. *Mol Biol Cell* 25(25):4010–4023
41. Wu Q, Shaikh MA, Meymand ES, Zhang B, Luk KC, Trojanowski JQ, Lee VM (2020) Neuronal activity modulates alpha-synuclein aggregation and

- spreading in organotypic brain slice cultures and in vivo. *Acta Neuropathol* 140(6):831–849
42. Fortin DL, Nemani VM, Voglmaier SM, Anthony MD, Ryan TA, Edwards RH (2005) Neural activity controls the synaptic accumulation of alpha-synuclein. *J Neurosci Off J Soc Neurosci* 25(47):10913–10921
 43. Diao J, Burre J, Vivona S, Cipriano DJ, Sharma M, Kyoung M, Sudhof TC, Brunger AT (2013) Native alpha-synuclein induces clustering of synaptic-vesicle mimics via binding to phospholipids and synaptobrevin-2/VAMP2. *eLife* 2:e00592
 44. Gao R, Asano SM, Upadhyayula S, Pisarev I, Milkie DE, Liu TL, Singh V, Graves A, Huynh GH, Zhao Y et al (2019) Cortical column and whole-brain imaging with molecular contrast and nanoscale resolution. *Science (New York, NY)* 363(6424):15900
 45. Karagiannis ED, Boyden ES (2018) Expansion microscopy: development and neuroscience applications. *Curr Opin Neurobiol* 50:56–63
 46. Kelly K, Wang S, Boddu R, Liu Z, Moukha-Chafiq O, Augelli-Szafran C, West AB (2018) The G2019S mutation in LRRK2 imparts resiliency to kinase inhibition. *Exp Neurol* 309:1–13
 47. Volpicelli-Daley LA, Luk KC, Lee VM (2014) Addition of exogenous alpha-synuclein preformed fibrils to primary neuronal cultures to seed recruitment of endogenous alpha-synuclein to Lewy body and Lewy neurite-like aggregates. *Nat Protoc* 9(9):2135–2146
 48. Roy S, Winton MJ, Black MM, Trojanowski JQ, Lee VM (2008) Cytoskeletal requirements in axonal transport of slow component-b. *J Neurosci Off J Soc Neurosci* 28(20):5248–5256
 49. Roy S, Winton MJ, Black MM, Trojanowski JQ, Lee VM (2007) Rapid and intermittent cotransport of slow component-b proteins. *J Neurosci Off J Soc Neurosci* 27(12):3131–3138
 50. Volpicelli-Daley LA (2017) Effects of alpha-synuclein on axonal transport. *Neurobiol Dis* 105:321–327
 51. Chen F, Tillberg PW, Boyden ES (2015) Optical imaging. *Expansion microscopy*. *Science (New York, NY)* 347(6221):543–548
 52. Sarkar D, Kang J, Wassie AT, Schroeder ME, Peng Z, Tarr TB, Tang A-H, Niederst E, Young JZ, Tsai L-H et al (2020) Expansion revealing: decrowding proteins to unmask invisible brain nanostructures. *bioRxiv* 20:12696
 53. Stoyka LE, Mahoney CL, Thrasher DR, Russell DL, Cook AK, Harris AT, Narayanan A, Janado TP, Standaert DG, Roberson ED et al (2021) Templated alpha-synuclein inclusion formation is independent of endogenous Tau. *eNeuro* 8(3):1205
 54. Lee SH, Valtschanoff JG, Kharazia VN, Weinberg R, Sheng M (2001) Biochemical and morphological characterization of an intracellular membrane compartment containing AMPA receptors. *Neuropharmacology* 41(6):680–692
 55. Taguchi K, Watanabe Y, Tsujimura A, Tanaka M (2019) Expression of alpha-synuclein is regulated in a neuronal cell type-dependent manner. *Anat Sci Int* 94(1):11–22
 56. West AB, Cowell RM, Daher JP, Moehle MS, Hinkle KM, Melrose HL, Standaert DG, Volpicelli-Daley LA (2014) Differential LRRK2 expression in the cortex, striatum, and substantia nigra in transgenic and nontransgenic rodents. *J Comp Neurol* 522(11):2465–2480
 57. Matikainen-Ankney BA, Kezunovic N, Mesias RE, Tian Y, Williams FM, Huntley GW, Benson DL (2016) Altered development of synapse structure and function in striatum caused by Parkinson's disease-linked LRRK2-G2019S mutation. *J Neurosci Off J Soc Neurosci* 36(27):7128–7141
 58. Chen C, Soto G, Dumrongprechachan V, Bannon N, Kang S, Kozorovitskiy Y, Parisiadou L (2020) Pathway-specific dysregulation of striatal excitatory synapses by LRRK2 mutations. *eLife* 9:102056
 59. Volta M, Beccano-Kelly DA, Paschall SA, Cataldi S, MacIsaac SE, Kuhlmann N, Kadgien CA, Tatarnikov I, Fox J, Khinda J et al (2017) Initial elevations in glutamate and dopamine neurotransmission decline with age, as does exploratory behavior, in LRRK2 G2019S knock-in mice. *eLife* 6:1059
 60. Fell MJ, Mirescu C, Basu K, Cheewatrakoolpong B, DeMong DE, Ellis JM, Hyde LA, Lin Y, Markgraf CG, Mei H et al (2015) MLI-2, a potent, selective, and centrally active compound for exploring the therapeutic potential and safety of LRRK2 kinase inhibition. *J Pharmacol Exp Ther* 355(3):397–409
 61. Sheng Z, Zhang S, Bustos D, Kleinheinz T, Le Pichon CE, Dominguez SL, Solanoy HO, Drummond J, Zhang X, Ding X et al (2012) Ser1292 autophosphorylation is an indicator of LRRK2 kinase activity and contributes to the cellular effects of PD mutations. *Sci Transl Med* 4(164):164ra161
 62. Chang JB, Chen F, Yoon YG, Jung EE, Babcock H, Kang JS, Asano S, Suk HJ, Pak N, Tillberg PW et al (2017) Iterative expansion microscopy. *Nat Methods* 14(6):593–599
 63. Dzamko N, Deak M, Hentati F, Reith AD, Prescott AR, Alessi DR, Nichols RJ (2010) Inhibition of LRRK2 kinase activity leads to dephosphorylation of Ser(910)/Ser(935), disruption of 14-3-3 binding and altered cytoplasmic localization. *Biochem J* 430(3):405–413
 64. Zhao Y, Dzamko N (2019) Recent developments in LRRK2-targeted therapy for Parkinson's disease. *Drugs* 79(10):1037–1051
 65. Benson DL, Matikainen-Ankney BA, Hussein A, Huntley GW (2018) Functional and behavioral consequences of Parkinson's disease-associated LRRK2-G2019S mutation. *Biochem Soc Trans* 46(6):1697–1705
 66. Ysselstein D, Nguyen M, Young TJ, Severino A, Schwake M, Merchant K, Krainc D (2019) LRRK2 kinase activity regulates lysosomal glucocerebrosidase in neurons derived from Parkinson's disease patients. *Nat Commun* 10(1):5570
 67. Martin I, Kim JW, Lee BD, Kang HC, Xu JC, Jia H, Stankowski J, Kim MS, Zhong J, Kumar M et al (2014) Ribosomal protein s15 phosphorylation mediates LRRK2 neurodegeneration in Parkinson's disease. *Cell* 157(2):472–485
 68. Orenstein SJ, Kuo SH, Tasset I, Arias E, Koga H, Fernandez-Carasa I, Cortes E, Honig LS, Dauer W, Consiglio A et al (2013) Interplay of LRRK2 with chaperone-mediated autophagy. *Nat Neurosci* 16(4):394–406
 69. Hur EM, Jang EH, Jeong GR, Lee BD (2019) LRRK2 and membrane trafficking: nexus of Parkinson's disease. *BMB Rep* 52(9):533–539
 70. Gcwenza NZ, Russell DL, Cowell RM, Volpicelli-Daley LA (2021) Molecular mechanisms underlying synaptic and axon degeneration in Parkinson's disease. *Front Cell Neurosci* 15:626128
 71. Boassa D, Berlanga ML, Yang MA, Terada M, Hu J, Bushong EA, Hwang M, Masliah E, George JM, Ellisman MH (2013) Mapping the subcellular distribution of alpha-synuclein in neurons using genetically encoded probes for correlated light and electron microscopy: implications for Parkinson's disease pathogenesis. *J Neurosci Off J Soc Neurosci* 33(6):2605–2615
 72. Clayton DF, George JM (1999) Synucleins in synaptic plasticity and neurodegenerative disorders. *J Neurosci Res* 58(1):120–129
 73. Maroteaux L, Campanelli JT, Scheller RH (1988) Synuclein: a neuron-specific protein localized to the nucleus and presynaptic nerve terminal. *J Neurosci Off J Soc Neurosci* 8(8):2804–2815
 74. Vargas KJ, Makani S, Davis T, Westphal CH, Castillo PE, Chandra SS (2014) Synucleins regulate the kinetics of synaptic vesicle endocytosis. *J Neurosci Off J Soc Neurosci* 34(28):9364–9376
 75. Kuhlmann N, Milnerwood AJ (2020) A critical LRRK at the synapse? The neurobiological function and pathophysiological dysfunction of LRRK2. *Front Mol Neurosci* 13(153):1609
 76. Beccano-Kelly DA, Kuhlmann N, Tatarnikov I, Volta M, Munsie LN, Chou P, Cao L-P, Han H, Tapia L, Farrer MJ et al (2014) Synaptic function is modulated by LRRK2 and glutamate release is increased in cortical neurons of G2019S LRRK2 knock-in mice. *Front Cell Neurosci* 8(301):1023
 77. Gurevicene I, Gurevicius K, Tanila H (2007) Role of alpha-synuclein in synaptic glutamate release. *Neurobiol Dis* 28(1):83–89
 78. Lee SK, Sillitoe RV, Silva C, Martina M, Sekerkova G (2015) alpha-Synuclein expression in the mouse cerebellum is restricted to VGLUT1 excitatory terminals and is enriched in unipolar brush cells. *Cerebellum (London, England)* 14(5):516–527
 79. Wang L, Das U, Scott DA, Tang Y, McLean PJ, Roy S (2014) alpha-synuclein multimers cluster synaptic vesicles and attenuate recycling. *Current Biol* 24(19):2319–2326
 80. Cheng F, Vivacqua G, Yu S (2011) The role of alpha-synuclein in neurotransmission and synaptic plasticity. *J Chem Neuroanat* 42(4):242–248
 81. Scott D, Roy S (2012) alpha-Synuclein inhibits intersynaptic vesicle mobility and maintains recycling-pool homeostasis. *J Neurosci Off J Soc Neurosci* 32(30):10129–10135
 82. Foffani G, Obeso JA (2018) A cortical pathogenic theory of Parkinson's disease. *Neuron* 99(6):1116–1128
 83. Marte A, Russo I, Rebosio C, Valente P, Belluzzi E, Pischedda F, Montani C, Lavarello C, Petretto A, Fedele E et al (2019) Leucine-rich repeat kinase 2 phosphorylation on synapsin I regulates glutamate release at pre-synaptic sites. *J Neurochem* 150(3):264–281
 84. Piccoli G, Condliffe SB, Bauer M, Giesert F, Boldt K, De Astis S, Meixner A, Sarioglu H, Vogt-Weisenhorn DM, Wurst W et al (2011) LRRK2 controls

- synaptic vesicle storage and mobilization within the recycling pool. *J Neurosci Off J Soc Neurosci* 31(6):2225–2237
85. Butler B, Saha K, Rana T, Becker JP, Sambo D, Davari P, Goodwin JS, Khoshbouei H (2015) Dopamine transporter activity is modulated by alpha-synuclein. *J Biol Chem* 290(49):29542–29554
 86. Artzi M, Even-Sapir E, Lerman SH, Thaler A, Urterger AO, Bressman S, Marder K, Hendler T, Giladi N, Ben BD et al (2017) DaT-SPECT assessment depicts dopamine depletion among asymptomatic G2019S LRRK2 mutation carriers. *PLoS one* 12(4):e0175424
 87. Longhena F, Faustini G, Missale C, Pizzi M, Bellucci A (2018) Dopamine transporter/alpha-synuclein complexes are altered in the post mortem caudate putamen of Parkinson's disease: an in situ proximity ligation assay study. *Int J Mol Sci* 19(6):10296
 88. Tang Y, Das U, Scott DA, Roy S (2012) The slow axonal transport of alpha-synuclein—mechanistic commonalities amongst diverse cytosolic cargoes. *Cytoskeleton (Hoboken, NJ)* 69(7):506–513
 89. Chevalier-Larsen E, Holzbaur EL (2006) Axonal transport and neurodegenerative disease. *Biochem Biophys Acta* 1762(11–12):1094–1108
 90. Deniston CK, Salogiannis J, Mathea S, Snead DM, Lahiri I, Matyszewski M, Donosa O, Watanabe R, Böhning J, Shiau AK et al (2020) Structure of LRRK2 in Parkinson's disease and model for microtubule interaction. *Nature* 588(7837):344–349
 91. Maday S, Twelvetrees AE, Moughamian AJ, Holzbaur EL (2014) Axonal transport: cargo-specific mechanisms of motility and regulation. *Neuron* 84(2):292–309
 92. Lis P, Burel S, Steger M, Mann M, Brown F, Diez F, Tonelli F, Holton JL, Ho PW, Ho SL et al (2018) Development of phospho-specific Rab protein antibodies to monitor in vivo activity of the LRRK2 Parkinson's disease kinase. *Biochem J* 475(1):1–22
 93. Seol W, Nam D, Son I (2019) Rab GTPases as physiological substrates of LRRK2 kinase. *Exp Neurobiol* 28(2):134–145
 94. Steger M, Diez F, Dhekne HS, Lis P, Nirujogi RS, Karayel O, Tonelli F, Martinez TN, Lorentzen E, Pfeffer SR et al (2017) Systematic proteomic analysis of LRRK2-mediated Rab GTPase phosphorylation establishes a connection to ciliogenesis. *eLife* 6:8742
 95. Steger M, Tonelli F, Ito G, Davies P, Trost M, Vetter M, Wachter S, Lorentzen E, Duddy G, Wilson S et al (2016) Phosphoproteomics reveals that Parkinson's disease kinase LRRK2 regulates a subset of Rab GTPases. *eLife* 5:120369

Publisher's Note

Springer Nature remains neutral with regard to jurisdictional claims in published maps and institutional affiliations.

Ready to submit your research? Choose BMC and benefit from:

- fast, convenient online submission
- thorough peer review by experienced researchers in your field
- rapid publication on acceptance
- support for research data, including large and complex data types
- gold Open Access which fosters wider collaboration and increased citations
- maximum visibility for your research: over 100M website views per year

At BMC, research is always in progress.

Learn more biomedcentral.com/submissions

